Gas Temperature Effect on Discharge-Mode Characteristics of Atmospheric-Pressure Dielectric Barrier Discharge in a Helium–Oxygen Mixture

Woo Seok Kang, Hyun-Su Kim, and Sang Hee Hong, *Member, IEEE*

***Abstract*—For a better understanding of gas temperature effects on plasma characteristics, a numerical study has been carried out for a dielectric barrier discharge (DBD) with a helium–oxygen mixture at atmospheric pressure. A one-dimensional time-dependent simulation code has been developed to solve continuity equations for plasma species and Poisson's equation for electric field calculation for a parallel-plate DBD reactor. To include temperature effects, gas heating by enthalpy change and Joule heating with ionic current movement are considered in the helium–oxygen plasma including 13 species reacting with one another according to 34 reactions depending on the gas temperature. Varying the ambient temperature from 300 K to 500 K, the plasma characteristics are calculated for the temporal variations and spatial distributions of electric field and species densities in the DBD region, and the different features of discharge modes are described by the voltage–current characteristic curves. A glowlike mode, which typically shows the formation of cathode fall, Faraday dark space, negative glow, and positive column in the spatial distributions of electric field and plasma density, is found in the discharge at a low ambient temperature, while a Townsend discharge mode with moderate electric field intensity and lower electron density is characterized at higher ambient temperatures. The temperature-dependent reactions strongly influence the generation and loss of species in the DBD plasma, and the decomposition of O_3 into O or O_2 and the quenching of metastable helium by the resultant O or O_2 play an important role in determining the distinct discharge mode in the DBD of a $He-O_2$ mixture. Furthermore, it is understood that the discharge-mode transition is controllable by the coupled effects of oxygen additive concentration, frequency, and gas temperature. A small amount of O_2 additive or a high-frequency operation exhibits a glow mode in a specific range of ambient temperature, of which reason can be explained by density variation and quenching of helium metastable species caused by the produced oxygen-related species.**

***Index Terms*—Atmospheric-pressure dielectric barrier discharge (DBD), discharge-mode characteristics, gas temperature effect, $He-O_2$ plasma, time-dependent simulation.**

I. Introduction

DIELECTRIC barrier discharge (DBD) has been used to generate nonequilibrium atmospheric-pressure plasmas in a few millimeters' gap between the electrodes that are covered with thin dielectric layers. The conventional application of DBD has been found typically in ozone production with spatially localized streamers [1], and recent studies for the generation of homogeneous DBD make it more attractive to produce abundant reactive species for various industrial fields [2]–[5].

The homogeneous DBD has two distinct discharge modes: glow and Townsend. The Townsend-mode DBD is characterized by small electric field distortion with low plasma density, while the glow-mode DBD exhibits high-density plasmas, which are more effective in materials processing. For this reason, current research interests have been mainly focused on understanding the mechanism of generation and sustenance of the glow DBD, and some specific control conditions are needed to maintain the glow mode. For the generation of glow DBD at atmospheric pressure, Kanazawa *et al.* [6] suggested three essential elements: helium as discharge gas, electrodes covered with dielectric barriers, and higher frequency power operation. Later, Massines *et al.* [3] verified experimentally that helium metastable species play dominant roles in generating and sustaining the glow mode in atmospheric-pressure helium discharge and extended their research to various discharge gas conditions [4]. From numerical simulation work, Gadri [7] showed that dielectric-barrier-controlled atmospheric-pressure glow discharges have the same characteristics to those of low-pressure dc glow discharges, for instance, high electric field distortions by a cathode sheath layer formation along with a nearly quasi-neutral positive column. Lee *et al.* [8] also simulated that the operation regimes for a glow mode of helium DBD could be determined by both oxygen additive concentration and applied power frequency. On the basis of these previous outcomes, it is emphasized that discharge reactor configuration, voltage and frequency of input power supply, and discharge gas species are the major factors influencing the generation and sustenance of a glow DBD.

However, in practice, when a DBD reactor is operated, gas temperature rise is usually accompanied because some part of the input electric power is inefficiently converted into heat over the entire electrodes and barriers enclosing the whole discharge volume. Moreover, the gas temperature in DBD can easily be varied because the reactor can be exposed to high or low ambient temperature in specific applications. In any cases, plasma characteristics are vulnerable to temperature changes, while plasma species react among them with the associated temperature-dependent reaction rates in a nonequilibrium

Manuscript received December 21, 2009; revised April 6, 2010; accepted May 13, 2010. Date of publication July 8, 2010; date of current version August 11, 2010. This work was supported in part by the Nuclear R&D Program and in part by the Brain Korea 21 Program through a National Research Foundation grant funded by the Korean government (MEST).

The authors are with the Department of Nuclear Engineering, Seoul National University, Seoul 151-742, Korea (e-mail: hongsh@snu.ac.kr).

Color versions of one or more of the figures in this paper are available online at http://ieeexplore.ieee.org.

Digital Object Identifier 10.1109/TPS.2010.2051238

plasma state. Such temperature change effects on DBD characteristics are also regarded as among the key issues for research to find optimum operational conditions for material surface treatment, which might be influenced by process parameters like gas temperature, gas flow, substrate temperature, etc., in atmospheric-pressure nonequilibrium plasma processing [9].

There have been numerous studies dealing with the issues on the effects of gas temperature in some types of atmospheric-pressure nonequilibrium plasmas. Among them, a gas temperature rise makes a breakdown voltage increase in corona discharge [10], and some plasma characteristics, such as electron density and electron temperature, are dependent on gas temperature in microwave plasmas [11]. In the case of DBD, there has also been the temperature issue that elevating the gas temperature decreases the ozone generation efficiency in an ozonizer [1], [12]. Moreover, it was reported that a temperature rise by gas heating could break the homogeneity of glowlike barrier discharge [13]. Even a recent experimental work showed temperature-dependent specific discharge patterns as the temperature decreased from room temperature to 88 K in a cryo-DBD [14]. Previous work showed that the temperature effect on DBD is evident, and more extensive research is essential for detailed analysis on temperature-dependent plasma characteristics in DBD.

In this numerical work, a one-dimensional (1-D) time-dependent simulation code for the atmospheric-pressure DBD in a helium–oxygen mixture is developed with temperature-dependent reactions among plasma species to understand temperature effects on DBD characteristics. The discharge characteristics of DBD are calculated under different ambient temperatures varying from 300 K to 500 K in a mixture of helium plasma gas and oxygen additive gas. The voltage–current characteristic curves of the discharge, which are suggested as a method to identify the feature of each discharge mode, are compared for the plasma modes in different temperature conditions. Additionally, the characteristics of DBD affected by other operating factors, such as O_2 additive concentration and RF frequency, are compared to find the influence of operating factors coupled with temperature on mode transition. Last, the importance of temperature control in the DBD reactor is examined as a case study.

II. Numerical Simulation

To simulate an atmospheric-pressure DBD, a 1-D time-dependent numerical study is carried out on the basis of a numerical code previously developed in the authors' research group [8], [15], [16]. In this simulation model for a 1-D DBD plasma, as shown in Fig. 1, the plasma is assumed to be uniformly distributed without any filamentary discharge in the computational domain of a parallel-plate DBD reactor with a 3-mm gap between the electrodes that are covered with dielectric materials of 1 mm in thickness with a relative permittivity (ε_r) of eight.

The motions of electrons and ions are calculated by continuity equations, and the electrostatic potential and electric field are obtained from Poisson's equation. For boundary conditions at the plasma–barrier interfaces, all the incoming fluxes of electrons or ions toward each barrier are assumed to be accumulated as surface charges depending on the electric field direction at the interfaces in the presence of secondary emission from the barrier surface and ion–electron recombination on the barrier

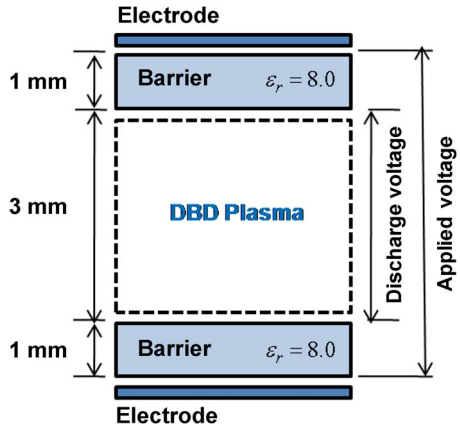

Fig. 1. Schematic diagram of a 1-D DBD computational domain used in this simulation.

$$\frac{\partial \sigma_i}{\partial t} = (1+\gamma_i) n_i v_i - \alpha_{re} \sigma_i \sigma_e$$

$$\frac{\partial \sigma_e}{\partial t} = n_e v_e - \alpha_{re} \sigma_i \sigma_e$$

where the subscripts i and e indicate the ion and the electron, respectively; σ is the accumulated surface charge density; γ (assumed to be 0.01) is the secondary emission coefficient from barrier surfaces; v is the drift velocity; n is the number density; and α_{re} (assumed to be 10^{-6}) is the ion–electron recombination coefficient over barrier surfaces. The boundary conditions for electric field and electric potential at the plasma–barrier interfaces are calculated from Gauss' theorem with surface charges [15].

To find the gas temperature, the energy equation, including enthalpy changes and Joule heating during the discharge, is adopted

$$\frac{\partial(\rho c_p T_g)}{\partial t} = -\nabla(-\kappa \nabla T_g + \rho v c_p T_g) + P \nabla \cdot v - \sum_i R_i \Delta H_i + \sum_i j_i \cdot E$$

where ρ is the total mass density, c_p is the heat capacity, κ is the thermal conductivity, v is the average gas velocity, P is the thermodynamic pressure, R_i is the rate coefficient of the ith reaction with the enthalpy change of H_i, and j_i is the current induced by the ith reaction listed in Table I. For the simplified 1-D calculation, the average gas velocity (v) is assumed to be externally controlled to be kept constant at 5 m/s over the whole discharge region by neglecting the boundary layer phenomena for the gas temperature calculation inside the discharge region. The ambient temperature is designated as the gas temperature at the barrier–plasma interface.

As the physical and chemical processes take place in the discharge gas, 34 reactions involving 13 helium- and oxygen-related species [He, $He(2^1S)$, $He(2^3S)$, He^+, He_2, $He_2(a^3\Sigma_u^+)$,

TABLE I
PHYSICAL AND CHEMICAL REACTIONS AND THEIR CORRESPONDING RATE COEFFICIENTS OF A HELIUM–OXYGEN MIXTURE IN THE DBD

i^{th}	Reaction	Rate coefficient (k_i)	Reference
1	$He + e \rightarrow He^+ + 2e$	$f(E/N)$	[17]
2	$He + e \rightarrow He(2^1S) + e$	$f(E/N)$	[17]
3	$He + e \rightarrow He(2^3S) + e$	$f(E/N)$	[17]
4	$He^* + 2He \rightarrow He_2(a^3\Sigma_u^+) + He$	$2.0 \times 10^{-34}\ cm^6 s^{-1}$	[20]
5	$He_2(a^3\Sigma_u^+) + He_2(a^3\Sigma_u^+) \rightarrow He_2^+ + 2He + e$	$1.5 \times 10^{-9}\ cm^3 s^{-1}$	[20]
6	$He_2(a^3\Sigma_u^+) + M \rightarrow 2He + M$	$1.0 \times 10^{6}\ s^{-1}$	[21]
7	$He^* + He^* \rightarrow He_2^+ + e$	$1.5 \times 10^{-9}\ cm^3 s^{-1}$	[20]
8	$He_2^+ + e \rightarrow He^* + He$	$8.9 \times 10^{-9}\ cm^3 s^{-1}$	[21]
9	$He^* + He^* \rightarrow He + He^+ + e$	$1.5 \times 10^{-9}(T_g/300)^{0.5}\ cm^3 s^{-1}$	[22]
10	$He + He^+ \rightarrow He + He^+$	$1.0 \times 10^{-9}(T_g/300)^{0.5}\ cm^3 s^{-1}$	[22]
11	$O_2 + e \rightarrow O_2^+ + 2e$	$f(E/N)$	[17]
12	$O_2^+ + e \rightarrow O + O$	$4.8 \times 10^{-7} cm^3 s^{-1}$	[17]
13	$O_2 + O^+ \rightarrow O_2^+ + O$	$2.0 \times 10^{-11}(T_g/300)^{-0.4}\ cm^3 s^{-1}$	[22]
14	$O_2^+ + e \rightarrow O_2^-$	$f(E/N)$	[17]
15	$O_3 + O \rightarrow O_2 + O_2$	$1.8 \times 10^{-11}\exp(-2300/T_g)\ cm^3 s^{-1}$	[23]
16	$O_2 + e \rightarrow O + O + e$	$2.0 \times 10^{-9} cm^3 s^{-1}$	[23]
17	$O_3 + e \rightarrow O + O_2 + e$	$5.0 \times 10^{-9}\ cm^3 s^{-1}$	[23]
18	$O + O + O_2 \rightarrow O_2 + O_2$	$3.8 \times 10^{-30}\exp(-170/T_g)/T_g\ cm^6 s^{-1}$	[23]
19	$O + O_2 + O \rightarrow O_3 + O$	$2.15 \times 10^{-34}\exp(345/T_g)\ cm^6 s^{-1}$	[23]
20	$O + O_2 + O_2 \rightarrow O_3 + O_2$	$6.9 \times 10^{-34}(300/T_g)^{1.25}\ cm^6 s^{-1}$	[23]
21	$O + O_2 + O_3 \rightarrow O_3 + O_3$	$4.6 \times 10^{-35}\exp(1050/T_g)\ cm^6 s^{-1}$	[23]
22	$O_3 + O_2 \rightarrow O + O_2 + O_2$	$7.3 \times 10^{-10}\exp(-11400/T_g)\ cm^3 s^{-1}$	[23]
23	$O_3 + O_3 \rightarrow O + O_2 + O_3$	$1.65 \times 10^{-9}\exp(-11400/T_g)\ cm^3 s^{-1}$	[23]
24	$O + O + O \rightarrow O_2 + O$	$9.21 \times 10^{-34} T_g^{-0.63}\ cm^6 s^{-1}$	[22]
25	$He^* + O_2 \rightarrow He + O_2^+ + e$	$2.54 \times 10^{-10}(T_g/300)^{0.5} cm^3 s^{-1}$	[22]
26	$He^* + O \rightarrow He + O^+ + e$	$2.54 \times 10^{-10}(T_g/300)^{0.5} cm^3 s^{-1}$	[22]
27	$He + O + O \rightarrow He + O_2$	$1.04 \times 10^{-33}\ cm^6 s^{-1}$	[24]
28	$He + O_2 + O \rightarrow He + O_3$	$3.4 \times 10^{-34} T_g^{-1.2}\ cm^6 s^{-1}$	[22]
29	$He + O_3 \rightarrow He + O_2 + O$	$2.28 \times 10^{-26}\ cm^3 s^{-1}$	[24]
30	$He^* + O_3 \rightarrow O_2^+ + O + He + e$	$2.54 \times 10^{-10}(T_g/300)^{0.5} cm^3 s^{-1}$	[22]
31	$He^+ + O_2 \rightarrow O^+ + O + He$	$1.07 \times 10^{-9}(T_g/300)^{0.5} cm^3 s^{-1}$	[22]
32	$He^+ + O_3 \rightarrow O^+ + O_2 + He$	$1.07 \times 10^{-9}(T_g/300)^{0.5} cm^3 s^{-1}$	[22]
33	$He^+ + O_2 \rightarrow O_2^+ + He$	$3.3 \times 10^{-11}(T_g/300)^{0.5} cm^3 s^{-1}$	[22]
34	$He^+ + O \rightarrow O^+ + He$	$5.0 \times 10^{-11}(T_g/300)^{0.5} cm^3 s^{-1}$	[22]

He_2^+, O, O^+, O_2, O_2^+, O_3, and electron] are listed in Table I, along with their rate coefficients that are dependent on the gas temperature. In this table, He^* represents the helium metastable-state species, i.e., $He(2^1S)$ and $He(2^3S)$, and T_g means the gas temperature in kelvins. A Boltzmann's equation solver, namely, BOLSIG+ [17], has been used for the calculation of electron energy distribution function (EEDF), i.e., $f(E/N)$. Then, the reaction rate coefficient, cross section, and electron mobility, which are dependent on electric field, are calculated from this EEDF. Moreover, the initial density of the neutral species is determined by the ideal gas law, i.e., $P = nkT$, including the gas temperature effect on density variations.

In the calculation of the electrical characteristics of the discharge, the discharge voltage between the dielectrics is

TABLE II
PARAMETER VALUES USED IN THIS NUMERICAL WORK

Geometrical Parameters			Input Power Parameters		Gas Parameters		Ambient Temperature
Barrier thickness	Barrier relative permittivity	Discharge gap distance	Applied voltage	Operation frequency	Plasma gas	Additive gas Concentration	
1 mm	8.0	3 mm	1.5 kV	10 ~ 30 kHz Sine wave	Helium (He)	Oxygen (O_2) 3 ~ 10 ppm	300 ~ 500 K

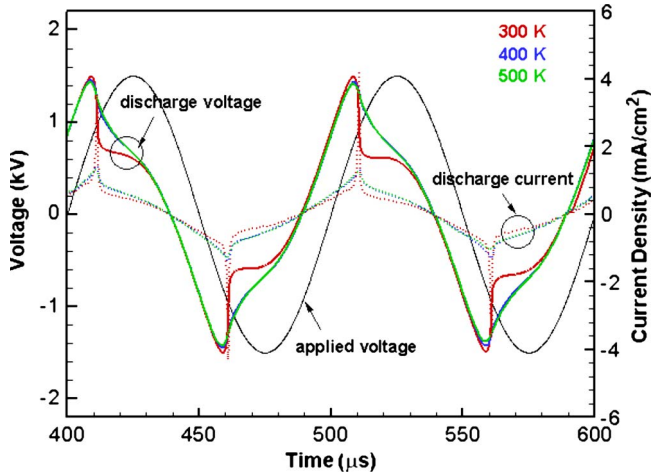

Fig. 2. Temporal variations of discharge voltages and currents responding to a sinusoidal applied voltage in the DBD reactor at different ambient temperatures (300 K, 400 K, and 500 K).

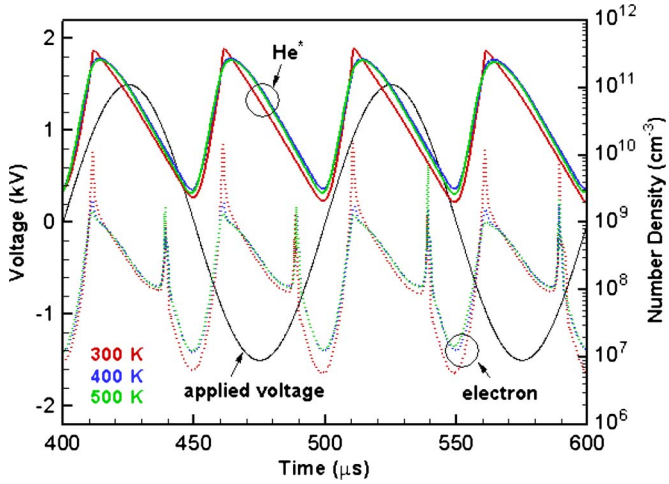

Fig. 3. Temporal variations of densities of electron and He* species responding to a sinusoidal applied voltage in the DBD reactor at different ambient temperatures (300 K, 400 K, and 500 K).

obtained, and the discharge current is calculated from the modified Sato's equation, including the time-dependent variations of the applied voltage [18]. A finite-difference method is taken as a numerical method associated with a flux-corrected transport (FCT) algorithm with upwind and Lax–Wendroff schemes [15], which are subsequently corrected by a numerical method suggested by Zalesak [19]. In Table II, all the parameter values used in this numerical work are summarized for geometry, input power, discharge gas, and ambient temperature.

III. SIMULATION RESULTS

A. *Effects of Ambient Temperature*

Simulations are carried out for DBD plasma characteristics under three different ambient temperatures of 300 K, 400 K, and 500 K at a fixed power frequency of 10 kHz and an oxygen additive concentration of 5 ppm. Figs. 2 and 3 show the temporal variations of electrical discharge characteristics and average densities of electron and helium metastable species (He^*), respectively, during two phases of a sinusoidal applied voltage.

In these figures, the repetitive profiles of discharge current, discharge voltage, and average species densities are found according to the applied voltage at different ambient temperatures. In Fig. 2 for 300 K, as the discharge voltage gradually increases up to a breakdown voltage of the gas, the discharge current slowly increases and then suddenly peaks up to a maximal current density of 4.2 mA/cm^2, which is followed by a large distortion of the discharge voltage in return with a rapid voltage drop. Such discharge patterns usually appear in the discharge characteristic profiles of typical atmospheric-pressure glow discharges [3], [8]. At the same moment of the current peak, the average densities of electrons and helium metastable species also exhibit their maximal values (1.0×10^{10} cm^{-3} for electron and 6.2×10^{11} cm^{-3} for He^*), as seen in Fig. 3. Meanwhile, at 400 K and 500 K in Figs. 2 and 3, small discharge current peaks of less than 1.4 mA/cm^2 are found with relatively moderate decreases in discharge voltages, and electron and He^* densities also show smaller peak values compared to those at 300 K (2.0×10^9 cm^{-3} for electron and 3.4×10^{11} cm^{-3} for He^*).

More distinguished characteristics according to ambient temperatures appear in the spatiotemporal distributions of electric field intensity (Fig. 4), electron density (Fig. 5), and He^* density (Fig. 6). When the discharge current reaches its peak value at ~ 510 μs or at ~ 560 μs in the 300-K condition, a strong electric field distortion occurs near each barrier, and accordingly, a high-density electron channel is formed in the whole discharge region. Moreover, high-density formation of He^* results in front of each barrier where a cathode fall region usually falls on. However, in the 500-K condition, the smaller electric field and electron density distributions are found, and the dispersed distributions of He^* densities appear over the discharge region with relatively lower densities.

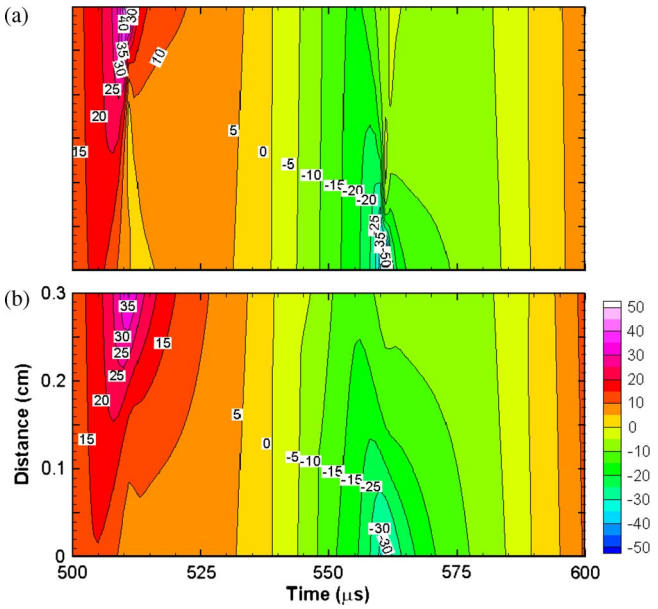

Fig. 4. Spatiotemporal variations of electric fields in the DBD reactor at different ambient temperatures: (a) 300 K and (b) 500 K (in kilovolts per centimeter).

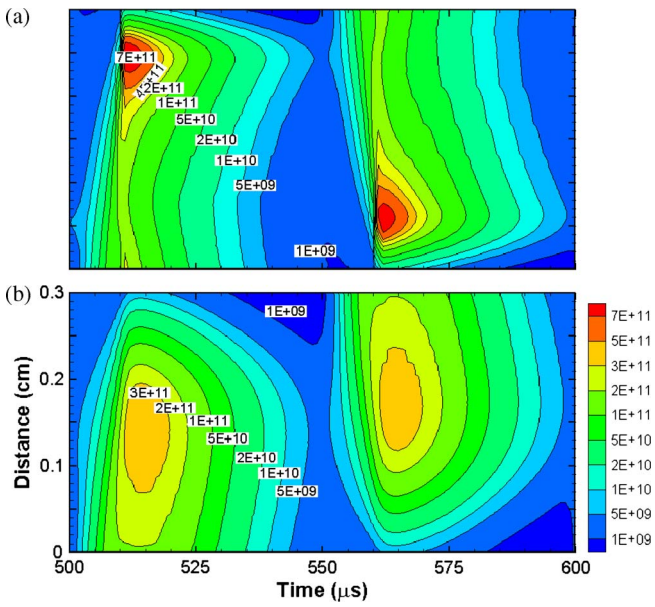

Fig. 6. Spatiotemporal variations of He* densities in the DBD reactor at different ambient temperatures: (a) 300 K and (b) 500 K (in cubic centimeters).

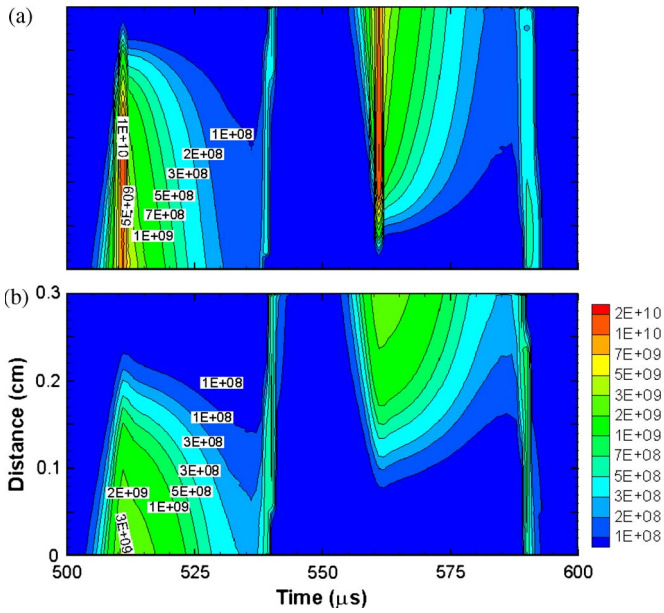

Fig. 5. Spatiotemporal variations of electron densities in the DBD reactor at different ambient temperatures: (a) 300 K and (b) 500 K (in cubic centimeters).

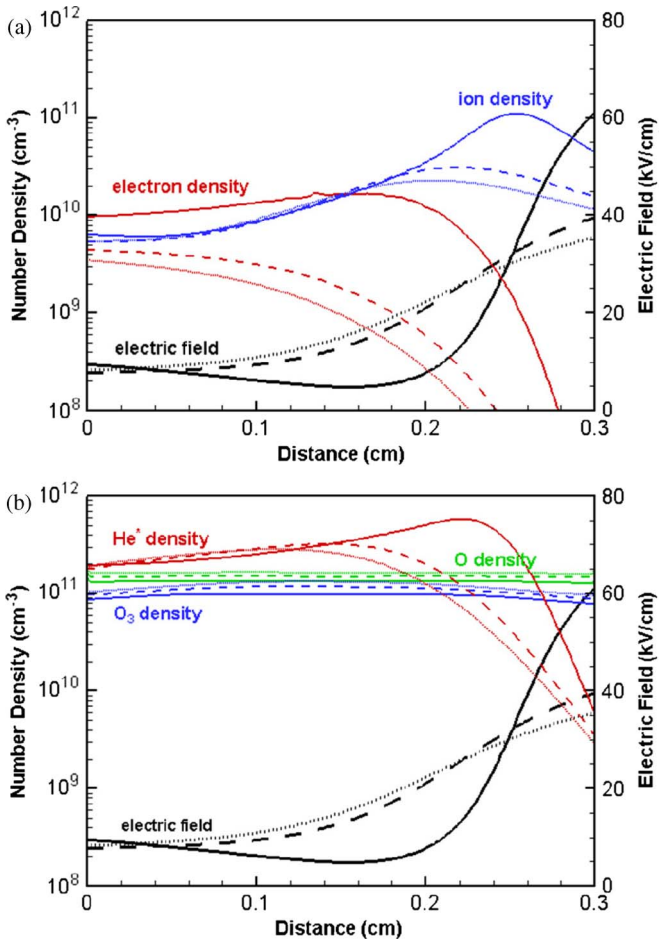

Fig. 7. Spatial distributions of species densities, along with electric field intensities at the peak currents in the DBD reactor at different ambient temperatures of (——) 300 K, (-----) 400 K, and (· · · · ·) 500 K: (a) electron and ion densities and (b) He*, O, and O_3 densities.

Fig. 7 more clearly shows the differences in the spatial distributions of electric field intensity and species densities at the moment of the peak discharge current in the DBD reactor among the three ambient temperature conditions. At 300 K, Fig. 7(a) shows the formation of cathode fall with high electric field (up to 62 kV/cm) near the cathode barrier, Faraday dark space, negative glow, and positive column in the spatial variations of electric field, and electron and ion densities. Such spatial plasma characteristics in the discharge region have also been found in the typical low-pressure dc glow discharge. Therefore, this plasma can be regarded as a glow discharge, which exhibits the same behaviors reported in the

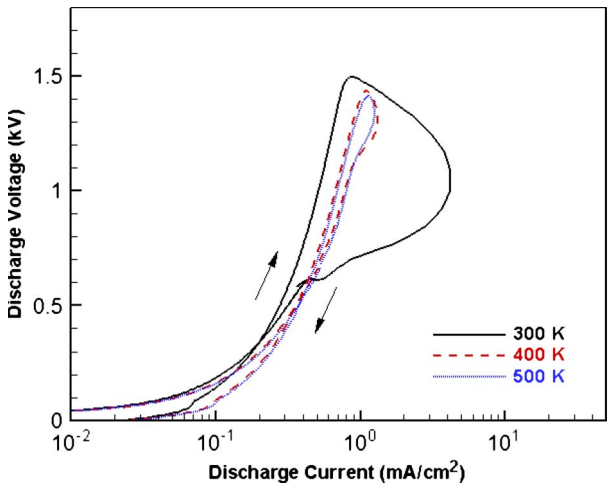

Fig. 8. Comparison of voltage–current characteristic curves during a half cycle of the sinusoidal applied voltage in the DBD reactor at different ambient temperatures of (——) 300 K, (-----) 400 K, and (· · · · · ·) 500 K.

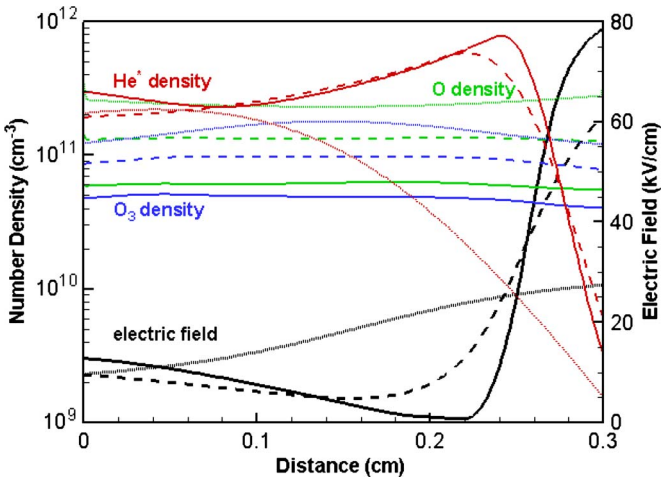

Fig. 9. Spatial distributions of He*, O, and O_3 densities, along with electric field intensities at the peak currents in the DBD reactor with different oxygen additive concentrations of (——) 3 ppm, (-----) 5 ppm, and (· · · · · ·) 10 ppm at 10 kHz and 300 K.

previous work dealing with a homogeneous glow DBD [3], [7], [8]. In particular, it is noted that the highest He* density of 6.2×10^{11} cm^{-3} is produced in this 300-K condition due to the formation of glow discharge at atmospheric pressure. On the other hand, at 400 K and 500 K, the Townsend-like discharge is characterized, as shown in Fig. 7, with moderate electric field intensities (< 40 kV/cm) and lower electron densities. It is also noticeable that He* density is lower, while O and O_3 densities are relatively higher at higher temperature.

As the various discharge modes, such as Townsend, glow, abnormal glow, and arc discharge, are distinguishable by their voltage–current (V–I) characteristic curves in the conventional low-pressure dc discharge [9], an attempt has been made to identify the exact discharge mode of the DBD by the calculated V–I characteristic curves. As shown in Fig. 8 for 300 K, the DBD plasma shows the typical characteristics of a self-sustaining glow discharge with increasing discharge currents up to 4.2 mA/cm^2, even during a descending phase of the discharge voltage (down to $\sim$1.1 kV). On the other hand, at 400 K and 500 K, the plasma cannot be sustained because the small discharge currents decreased in the voltage drop phase.

B. Effects of Oxygen Additive and Power Frequency Coupled With Gas Temperature

It was previously revealed that the effects of oxygen additive and frequency play an import role in the determination of discharge mode between Townsend and glow [3], [8]. In order to find out in detail the effects of these factors along with temperature, calculations are carried out in the cases of different amounts of oxygen additive and changes of frequency.

To find the effects of oxygen additive in the helium plasma, the amounts of O_2 concentration are varied with 3, 5, and 10 ppm at 10 kHz and 300 K. The calculated results for different oxygen concentrations are compared in Fig. 9 for the spatial distributions of electric field and species densities. At low amounts of oxygen (3 and 5 ppm), higher He* densities (up to 7.7×10^{11} cm^{-3}) are found near the cathode fall region in a glowlike discharge. However, when an excessive O_2 (10 ppm) is added, the discharge shows a Townsend mode with low He* densities ($< 2.1 \times 10^{11}$ cm^{-3}) and relatively higher densities of O and O_3. This can be explained that the excessive O_2 addition makes the densities of oxygen-related species (like O, O_2, and O_3) increase, and these species, in turn, quench the production of helium metastable species. The changes of discharge modes with the O_2 additive concentration are more apparent in the V–I characteristic curves shown in Fig. 11(a), where the glow and Townsend modes are clearly distinguished between the O_2 concentrations of 3 and 10 ppm.

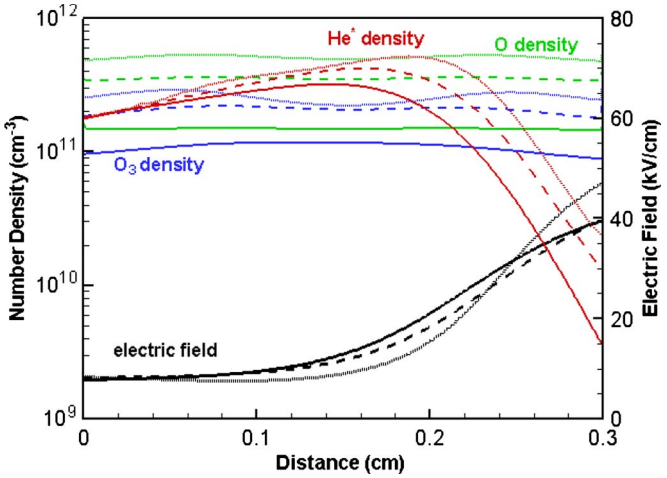

Fig. 10. Spatial distributions of He*, O, and O_3 densities, along with electric field intensities at the peak currents in the DBD reactor for different frequencies of (——) 10 kHz, (-----) 20 kHz, and (· · · · · ·) 30 kHz at 300 K and 5 ppm.

Additional calculations are carried out to understand the frequency effects for 10, 20, and 30 kHz at 5-ppm oxygen additive and 400-K ambient temperature. As the result shows in Fig. 10, the DBD operation with a higher frequency at 30 kHz produces relatively higher species densities (5.1×10^{11} cm^{-3} for He*, 5.2×10^{11} cm^{-3} for O, and 2.8×10^{11} cm^{-3} for O_3), and it is presumed that the higher frequency operation

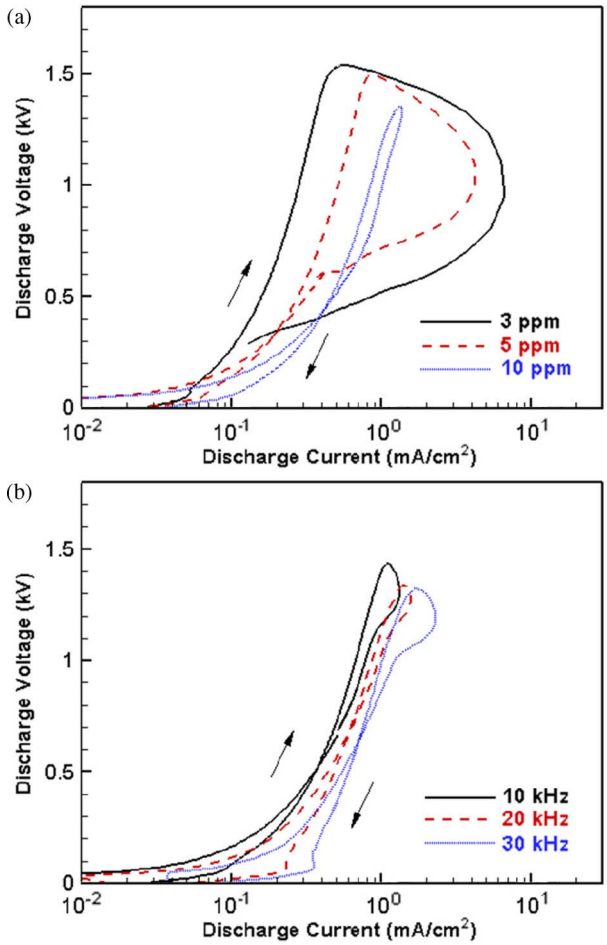

Fig. 11. Comparison of voltage–current characteristic curves during a half cycle of the sinusoidal applied voltage in the DBD reactor. (a) For different oxygen additives of (——) 3 ppm, (-----) 5 ppm, and (· · · · · ·) 10 ppm, and (b) for different frequencies of (——) 10 kHz, (-----) 20 kHz, and (· · · · · ·) 30 kHz at 400 K and 5 ppm.

also makes electron density and discharge current increase to sustain a glowlike discharge. The V–I characteristic curves shown in Fig. 11(b) exhibit that the higher frequency operation tends to make the maximum discharge current increase with the decrease of the discharge-sustaining voltage.

IV. Discussion

The simulation results show that the discharge characteristics in DBD are strongly influenced by the gas temperature. The gas temperature is considered to affect the concentrations of the species to increase or decrease through the temperature-dependent reactions listed in Table I for an atmospheric-pressure DBD of $He-O_2$ mixture gas. The mechanism of the mode transition from glow to Townsend due to the temperature rise can be explained by the following two-step reactions. In the first step, some temperature-dependent reaction rate coefficients increase at a high ambient temperature, and the dissociation of ozone is accordingly accelerated by the relevant reactions in Table I, such as

$$O_3 + O_2 \rightarrow O + O_2 + O_2 \quad \text{with } k_{22} = 7.3 \times 10^{-10} \exp(-11400/T_g)\ \text{cm}^3 \cdot \text{s}^{-1}$$

or

$$O_3 + O_3 \rightarrow O + O_2 + O_3 \quad \text{with } k_{23} = 1.65 \times 10^{-9} \exp(-11400/T_g)\ \text{cm}^3 \cdot \text{s}^{-1}.$$

Hence, the density of ozone reduces, while the densities of O and O_2 increase in the discharge region. In the second step, these increased O and O_2 species quench the generation of He^* species that are necessary to sustain a glow discharge state, and therefore, the density of He^* decreases so that the discharge characteristics will be readily changed to a Townsend mode.

In a similar manner, the discharge-mode transition can also be explained by the generation and reduction of the helium metastable species affected by other factors, such as oxygen additive and frequency, as shown in Fig. 12 with a schematic diagram of the physical mechanism determining a discharge mode in DBD by control of O_2 additive, frequency, and gas temperature. In the case of oxygen additive control, a large amount of oxygen additive results in the generation of high density of O and O_2, which, in turn, quench the He^* generation to lead the discharge eventually to a Townsend mode. On the other hand, in the case of frequency change, increasing the frequency enhances the electric field intensity and electron density, which generate much more He^* species in the whole discharge region exhibiting a glowlike mode.

As the discharge mode is determined by the coupled effects of the three factors (not only by a single one), it is hard to control the discharge mode affected by an individual factor in a certain condition. The previous authors' work reported the discharge modes determined by the coupled effects of the two factors, namely, O_2 additive and frequency [8]. In addition to these two factors, the mode transition between glow and Townsend can be characterized by the coupled three factors, i.e., O_2 additive, frequency, and ambient temperature. In Fig. 13, the three mode transition regimes, called as *zones A*, *B*, and *C*, are separated according to the operating values of ambient temperature and frequency, and the discharge mode in each zone is determined by the value of O_2 concentration. For a glow (or Townsend) discharge mode, the O_2 concentration should be larger (or smaller) than the critical one.

When focusing only on the temperature effect on the discharge mode, it is inferred that the temperature control of a DBD reactor is important to minimize the unintended change of discharge characteristics in any ambient or internal circumstances. In order to illustrate such a situation, the effects of electrode barrier cooling on the discharge mode are shown in Fig. 14. The ambient and inlet gas temperatures are initially kept at 400 K for the DBD, and then, three cooling cases are considered: 1) no barrier cooling; 2) barrier cooling down to 350 K; and 3) barrier cooling down to 300 K, as shown in Fig. 14(a). The different discharge characteristics are compared by the V–I characteristic curves shown in Fig. 14(b), in which the discharge without cooling shows a Townsend mode, but the discharge characteristics are gradually changed to a glow mode with lowering the barrier temperature by cooling. These results suggest that the discharge feature can be maintained or controlled for a homogeneous glow mode, even in an elevated ambient or gas temperature condition by a well-controlled heat

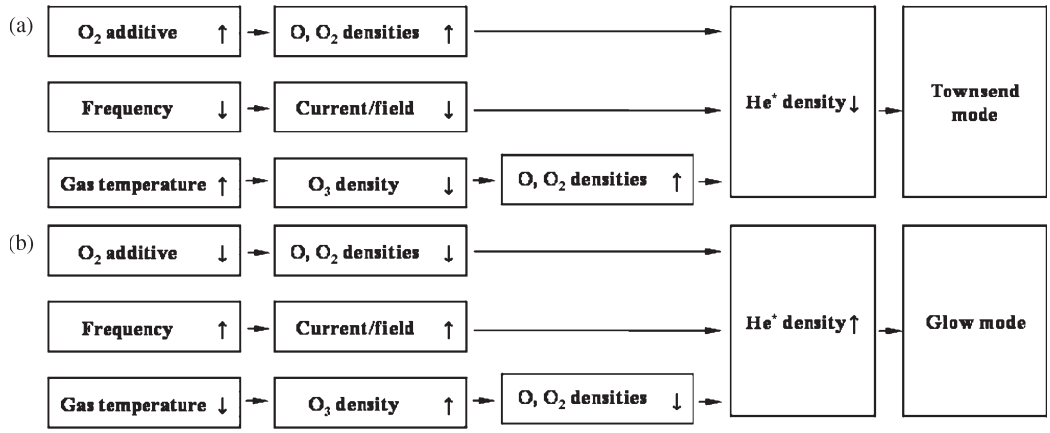

Fig. 12. Schematic diagrams describing the physical mechanisms of the discharge mode determined by control of oxygen additive, frequency, and gas temperature for the DBD. (a) Townsend mode. (b) Glow mode.

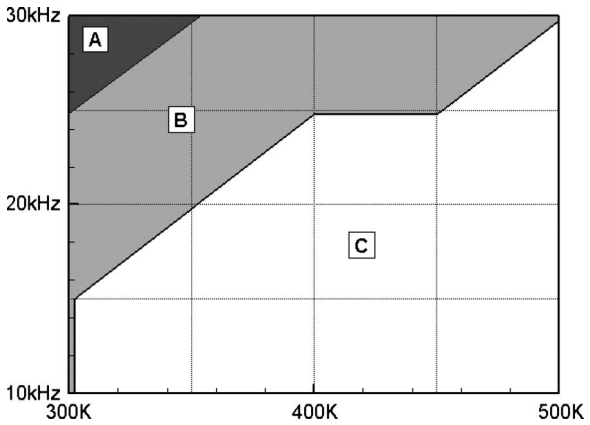

Fig. 13. Discharge-mode transition zones appeared in the temperature-frequency parameter space, which are characterized by the amount of oxygen additive. In each zone, a mode transition between glow and Townsend takes place at a critical O_2 concentration (7 ppm in *zone A*, 5 ppm in *zone B*, and 3 ppm in *zone C*). If the O_2 concentration is greater than the critical one, the discharge exhibits a glow mode; otherwise, it exhibits a Townsend mode.

removal design of the DBD reactor, including electrode-cooling components, barrier material options, and control of input gas temperature and flow rate.

V. Conclusion

A 1-D time-dependent simulation for the atmospheric-pressure DBD has been developed by taking account of temperature-dependent reactions in a $He-O_2$ mixture plasma. The calculated results have been obtained for the temporal variations and spatial distributions of the discharge characteristics, such as electric field, electron density, and ion and radical species densities. The different discharge characteristics of glow and Townsend modes have been described and compared by the discharge voltage–current characteristic curves.

The effects of gas temperature on discharge characteristics have been numerically simulated for a frequency of 10 kHz and an O_2 additive concentration of 5 ppm. At low ambient temperature (300 K), a glowlike mode is characterized in the DBD with high values of discharge current, electron and He^* densities, and electric field intensity. On the contrary, at high ambient temperature (400 K or 500 K), a Townsend discharge

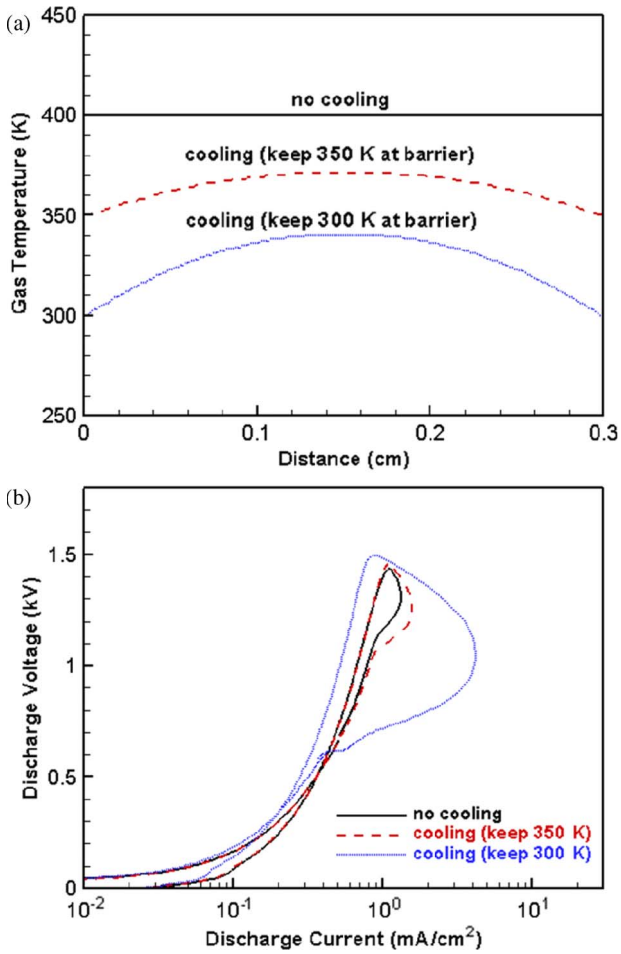

Fig. 14. Effects of electrode barrier cooling (a) on temperature profiles inside the DBD region and (b) on discharge voltage–current characteristic curves for 10 kHz and 5 ppm.

mode is featured with the reduced values of discharge current, electron and He^* densities, and electric field intensity. The mode characteristics are also analyzed by the voltage–current characteristic curves, and the different discharge characteristics caused by ambient temperature changes suggest that the temperature-dependent reactions strongly influence the generation and loss of species in the DBD plasma.

The coupled influences of frequency and temperature, along with O_2 concentration on mode transition characteristics, have been analyzed, and the schematic diagrams of the physical mechanisms and transition zones for the discharge modes have been presented. A small amount of O_2 additive or a high-frequency operation shows a glow mode in a specific range of ambient temperature, whose reason is explained by the density variation and quenching of helium metastable species caused by the produced oxygen-related species. It is understood from the mode transition zones suggested herein that the transition phenomena between glow and Townsend modes are controllable not by a single factor but by the coupled factors of O_2 additive, frequency, and gas temperature. Calculations for different cooling cases predict that the discharge mode can be determined by temperature control through boundary cooling and that a proper cooling design of the DBD reactor has to be supplemented to generate and sustain a stable homogeneous DBD.

REFERENCES

[1] B. Eliasson, M. Hirth, and U. Kogelschatz, "Ozone synthesis from oxygen in dielectric barrier discharges," *J. Phys. D, Appl. Phys.*, vol. 20, no. 11, pp. 1421–1437, Nov. 1987.

[2] U. Kogelschatz, "Filamentary, patterned, and diffuse barrier discharges," *IEEE Trans. Plasma Sci.*, vol. 30, no. 4, pp. 1400–1408, Aug. 2002.

[3] F. Massines, A. Rabehi, P. Decomps, R. B. Gadri, P. Segur, and C. Mayoux, "Experimental and theoretical study of a glow discharge at atmospheric pressure controlled by dielectric barrier," *J. Appl. Phys.*, vol. 83, no. 6, pp. 2950–2957, Mar. 1998.

[4] F. Massines, N. Gherardi, N. Naude, and P. Segur, "Glow and townsend dielectric barrier discharge in various atmosphere," *Plasma Phys. Control. Fusion*, vol. 47, no. 12B, pp. 577–588, Nov. 2005.

[5] T. C. Montie, K. Kelly-Wintenberg, and J. R. Roth, "An overview of research using the one atmosphere uniform glow discharge plasma (OAUGDP) for sterilization of surfaces and materials," *IEEE Trans. Plasma Sci.*, vol. 28, no. 1, pp. 41–50, Feb. 2000.

[6] S. Kanazawa, M. Kogoma, T. Moriwaki, and S. Okazaki, "Stable glow plasma at atmospheric pressure," *J. Phys. D, Appl. Phys.*, vol. 21, no. 5, pp. 838–840, May 1988.

[7] R. B. Gadri, "One atmosphere glow discharge structure revealed by computer modeling," *IEEE Trans. Plasma Sci.*, vol. 27, no. 1, pp. 36–37, Feb. 1999.

[8] D. Lee, J. M. Park, S. H. Hong, and Y. Kim, "Numerical simulation on mode transition of atmospheric dielectric barrier discharge in helium–oxygen mixture," *IEEE Trans. Plasma Sci.*, vol. 33, no. 2, pp. 949–957, Apr. 2005.

[9] J. R. Roth, *Industrial Plasma Engineering*. London, U.K.: IOP, 1995.

[10] H. S. Uhm, S. J. Jung, and H. S. Kim, "Influence of gas temperature on electrical breakdown in cylindrical electrodes," *J. Korean Phys. Soc.*, vol. 42, pp. S989–S993, 2003.

[11] L. XinPei, "Effects of gas temperature and electron temperature on species concentration of air plasmas," *J. Appl. Phys.*, vol. 102, no. 3, p. 033 302, Aug. 2007.

[12] J. Ozonek, S. Fijalkowski, and J. Czerwi, "Thermodynamic aspects of equilibrium ozone generation," *Plasma Process. Polym.*, vol. 4, no. 7/8, pp. 701–709, 2007.

[13] Y. B. Golubovskii, V. A. Maiorov, J. Behnke, and J. F. Behnke, "On the stability of a homogeneous barrier discharge in nitrogen relative to radial perturbations," *J. Phys. D, Appl. Phys.*, vol. 36, no. 8, pp. 975–981, Apr. 2003.

[14] J. H. Choi, Y. Noma, T. Tomai, and K. Terashima, "Temperature-dependent transition of discharge pattern of He/air cryoplasma," *Appl. Phys. Lett.*, vol. 93, no. 8, p. 081 504, Aug. 2008.

[15] W. S. Kang, J. M. Park, Y. Kim, and S. H. Hong, "Numerical study on influences of barrier arrangements on dielectric barrier discharge characteristics," *IEEE Trans. Plasma Sci.*, vol. 31, no. 4, pp. 504–510, Aug. 2003.

[16] Y. Kim, W. S. Kang, J. M. Park, S. H. Hong, Y.-H. Song, and S. J. Kim, "Experimental and numerical analysis of streamers in pulsed corona and dielectric barrier discharges," *IEEE Trans. Plasma Sci.*, vol. 32, no. 1, pp. 18–24, Feb. 2004.

[17] G. J. M. Hagelaar, BOLSIG+: User-Friendly Solver for Electron Boltzmann Equation, 2008. [Online]. Available: http://www.laplace.univ-tlse.fr

[18] R. Morrow and N. Sato, "The discharge current induced by the motion of charged particles in time-dependent electric fields; Sato's equation extended," *J. Phys. D, Appl. Phys.*, vol. 32, no. 5, pp. L20–L22, Mar. 1999.

[19] S. T. Zalesak, "Fully multidimensional flux-corrected transport algorithms for fluids," *J. Comput. Phys.*, vol. 31, no. 3, pp. 335–363, Jun. 1979.

[20] R. Deloche, P. Monchicourt, M. Cheret, and F. Lambert, "High-pressure helium afterglow at room temperature," *Phys. Rev. A, Gen. Phys.*, vol. 13, no. 3, pp. 1140–1176, Mar. 1976.

[21] Y. B. Golubovskii, V. A. Maiorov, J. Behnke, and J. F. Behnke, "Modelling of the homogeneous barrier discharge in helium at atmospheric pressure," *J. Phys. D, Appl. Phys.*, vol. 36, no. 1, pp. 39–49, Jan. 2003.

[22] D. S. Stafford and M. J. Kushner, " $O_2(^1\Delta)$ production in He/O_2 mixtures in flowing low pressure plasmas," *J. Appl. Phys.*, vol. 96, no. 5, pp. 2451–2465, Sep. 2004.

[23] R. Peyrous, P. Pignolet, and B. Held, "Kinetic simulation of gaseous species created by an electrical discharge in dry or humid oxygen," *J. Phys. D, Appl. Phys.*, vol. 22, no. 11, pp. 1658–1667, Nov. 1989.

[24] J. Y. Jeong, J. Park, I. Henins, S. E. Babayan, V. J. Tu, G. S. Selwyn, G. Ding, and R. F. Hicks, "Reaction chemistry in the afterglow of an oxygen–helium, atmospheric-pressure plasma," *J. Phys. Chem. A*, vol. 104, no. 34, pp. 8027–8032, Aug. 2000.

Woo Seok Kang received the B.S. and M.S. degrees in nuclear engineering from Seoul National University, Seoul, Korea, in 2000 and 2002, respectively, where he is currently working toward the Ph.D. degree in the Department of Nuclear Engineering.

From 2002 to 2004, he was with the Korea Institute of Science and Technology Evaluation and Planning, Seoul, where he managed national nuclear R&D programs. In 2004, he joined Samsung Corning Company, Ltd. and was involved in R&D projects for next-generation liquid crystal display technologies. His research interests include the diagnosis and simulation of atmospheric pressure plasmas for materials processing.

Hyun-Su Kim was born in Busan, Korea, in 1982. He received the B.S. and M.S. degrees in nuclear engineering from Seoul National University, Seoul, Korea, in 2006 and 2008, respectively, where he is currently working toward the Ph.D. degree in the Department of Nuclear Engineering.

His research interests are focused on the application of atmospheric-pressure barrier discharge and thermal plasma sources.

Sang Hee Hong (M'87) received the B.S. degree in applied physics from Seoul National University, Seoul, Korea, in 1974 and the M.S. and Ph.D. degrees in electrical engineering from Colorado State University, Fort Collins, in 1975 and 1978, respectively.

In 1979, he joined Seoul National University, where he is currently a Professor in the Department of Nuclear Engineering. He spent a year at the University of Sydney, Sydney, Australia, in 1989 as a Visiting Professor. His principal areas of research in the U.S. and Australia were the stability analysis of MHD flows and the theory of rotating plasmas and plasma centrifuges. Recently, his research work has included the tokamak transport modeling and the development of thermal and nonequilibrium plasma sources, along with their applications to material and environmental processing. His research interests in Korea moved to the numerical modeling of tokamak plasmas and industrial processing plasmas.